Received: 17 December 2021 | Revised: 26 April 2022 | Accepted: 4 May 2022

DOI: 10.1002/ese3.1186

ORIGINAL ARTICLE

Analysis and assessment of a novel organic flash Rankine cycle (OFRC) system for low-temperature heat recovery

Qi Wang[1] | **Rafael Macián-Juan**[1] | **Dantong Li**[2]

[1]Department of Energy & Process Engineering, School of Engineering and Design, Technical University of Munich (TUM), Garching, Germany

[2]Department of Compressor Engineering, School of Energy and Power Engineering, Xi'an Jiaotong University, Xi'an, China

Correspondence
Qi Wang, Department of Energy & Process Engineering, School of Engineering and Design, Technical University of Munich (TUM), 85748 Garching, Germany.
Email: qi.wang@tum.de

Funding information
China Scholarship Council, Grant/Award Number: 202006280024

Abstract

In this paper, a novel organic flash Rankine cycle (OFRC) system for low-temperature heat recovery is analyzed and optimized using the 3E (energy, exergy, and economic) analysis method and particle swarm optimization algorithm, respectively. Five environmentally friendly organic fluids and three typical heat source conditions are simultaneously discussed during the parametric analysis and optimization process, to obtain a comprehensive understanding of the thermo-economic characteristics of this novel system. The main analysis results show that the biggest exergy loss of the OFRC system is caused by the condenser, followed by the evaporator. About 70% of the specific power cost is caused by the capital investment of the system, and more than 60% of the capital investment is spent on purchasing the high-pressure and low-pressure expanders. Under the same operating conditions, the working fluids with high critical temperatures can achieve higher cycle thermal efficiency and lower specific power costs than those with low critical temperatures. The optimization results show that the OFRC system is able to achieve a better thermodynamic performance than the organic Rankine cycle (ORC) and organic flash cycle (OFC) systems, and when the heat source's inlet temperature is set to 100°C, 120°C, and 140°C, R245fa, R290, and R152a are, respectively, recommended as the best working fluid for the OFRC system. Besides this, it is found that the OFC system has the worst thermo-economic performance, and the ORC system can achieve the lowest specific power cost. A new finding is that, for all three systems, the higher the critical temperature of the working fluid, the lower the specific power cost of the system.

KEYWORDS

low-temperature heat recovery, organic flash cycle, organic Rankine cycle, particle-swarm optimization, thermo-economic analysis

1 | INTRODUCTION

Nowadays, research on waste heat recovery technology has attracted more and more attention due to the decreasing fossil fuel storage and severe environmental problems. The organic Rankine cycle (ORC) employing organic fluids as the working fluid is considered an outstanding waste heat recovery technology as it shows great potential in converting the low-grade thermal energy to mechanical or electrical energy.[1–3] Currently, the ORC is being widely used for low-temperature heat recovery and renewable energy exploitation owing to its excellent characteristics of compact system configuration, autonomous operation, and low investment and maintenance costs.[4,5]

The basic ORC and the regenerative ORC are two most common cycle architectures, which have been actively studied by many researchers from both aspects of experiment and simulation. For instance, Zhang et al.[6] conducted an experimental study of these two systems under different heating and cooling conditions. The results showed that, for the heat sources with low temperatures, the basic ORC could achieve a better system performance than the regenerative ORC. However, the regenerative ORC would be more suitable for the exploitation of high-temperature heat sources. Feng et al.[7] conducted a performance comparison of the regenerative ORC and the basic ORC, based on the non-dominated sorting genetic algorithm (NSGA). It was reported that under the Pareto-optimal condition, the exergy efficiency of the regenerative ORC was 8.1% higher than that of the basic ORC. In addition, it was also found that, for both cycles, the cycle's highest thermal and exergy efficiencies were always achieved with the worst economic performance and the smallest net electrical power output.[7] Besides, in the evaporators of the two cycles, a poor temperature matching between the heat source and the working fluid is caused by the isothermal evaporation process, which eventually leads to a big exergy loss.[8] Thus, these two cycles have difficulty in achieving high exergy efficiency. To solve this problem, many promising approaches such as the supercritical ORC,[9] the ORC using zeotropic mixtures,[10] the trilateral flash cycle (TFC),[11] the organic flash cycle (OFC),[12] the multi-stage ORC[13–16], and the combined cycle[17,18] have been proposed in the published papers.

The supercritical ORC was considered as an effective solution in improving the system performance and reducing the exergy loss of the heat recovery process as it could avoid the undesirable isothermal evaporation process taking place in the two-phase region.[19] Furthermore, the supercritical ORC operating with high temperatures and pressures was able to achieve a higher system efficiency than the subcritical ORC when a recuperator was used.[20] The high pressures of the supercritical conditions however limited the development of this technology.[21] To decrease the exergy loss of the heat recovery process but with a moderate operating pressure, the ORC using zeotropic mixtures was proposed and investigated.[22] As a better temperature matching was achieved in the evaporator, the zeotropic ORC could obtain a higher exergy efficiency.[23] However, some issues including the uncertainty of fluid properties, the unknown heat transfer coefficients, and the composition determination of working fluids still exist in practical applications, confining the spread of this cycle.[24] The TFC proposed by Smith et al. in 1993[11] was considered the cycle with the best temperature matching due to its 100% single-phase heating process. Therefore, for the low-temperature heat recovery, the TFC showed great potential in obtaining high system efficiencies.[25] For instance, Yari et al.[26] conducted a comparison study of the thermo-economic performance of the TFC, ORC, and Kalina cycle. It was found that under a low-temperature heat source of 120°C, the TFC could achieve a larger net power output than both the ORC and Kalina cycle. However, it was also concluded that the thermo-economic performance of the TFC was strongly affected by the isentropic efficiency of the two-phase expander. It should be emphasized that the expansion process in the TFC expander is a two-phase flash expansion whose thermodynamic characteristics differ significantly from the conventional gas expansion.[25] According to the papers of Bianchi et al.[27] and Wang et al.,[28] a major problem with the TFC is the design and manufacture of a reliable and efficient two-phase expander, which greatly limits the applications of this technology. To date, only several conceptual TFC systems have been experimentally tested.[29]

As an improved version of the TFC, the OFC is another well-known low-temperature heat recovery cycle, which has been actively studied for geothermal energy exploitation. Different from the TFC, in the OFC, the saturated liquid at the heater outlet is first flashed into the vapor–liquid two-phase mixture via a throttle valve, and then, the flashed vapor is introduced into a conventional gas expander.[30] Although the exergy loss of the heat recovery process is reduced, this benefit has been negated by the additional exergy loss caused by the throttling process.[12] So far, several methods have been proposed to improve the efficiency of the basic OFC system. For instance, Ho et al.[31] proposed four design improvements in both the cycle layout and configuration. The obtained results showed that a higher system efficiency could be achieved by replacing the throttling valve with a two-phase expander. To lower the exergy loss of the throttling process as much as possible, Chen et al.[32] proposed to apply ejectors

to three OFC systems with different cycle configurations. It was concluded that these ejector-based OFC systems could achieve high system efficiencies and had the potential for moderate-to-low grade waste heat recovery. To decrease the heat exchanger size and save the investment cost, Baccioli et al.[30] proposed a regenerative OFC with the ability to recover waste heat from the liquid at the outlet of the flash tank (or flash evaporator). Meng et al.[33] analyzed and compared four different regenerative OFCs driven by the geothermal water with temperatures of 120°C to 180°C. They found that all four regenerative OFCs could achieve larger net power output and higher thermal and exergy efficiencies than the basic OFC. In addition, Meng et al.[34] conducted a comparison study of three improved organic double-flash cycles (ODFCs) with regenerator or two-phase expander. The investigation results showed that compared to the basic ODFC, these improved ODFCs could obtain higher system efficiencies while achieving a lower Levelized cost of electricity.

In addition to the above-mentioned cycle improvement methods, the multi-stage cycle and the combined cycle are another two effective solutions for enhancing the thermodynamic performance of the system, which have received growing attention in recent years. For instance, Sun et al.[13] investigated a dual-pressure ORC system driven by geothermal energy, and they found that the dual-pressure ORC system could achieve a better thermodynamic performance than the conventional single-pressure ORC system. Shu et al.[15] conducted a theoretical study on a dual-loop ORC system that consists of two ORC loops with different operating temperatures. Using two ORC loops, the energy cascade utilization principle could be achieved and the system efficiencies were improved. Rashwan et al.[16] performed a thermodynamic analysis of a novel cascaded closed loop type ORC, and they found that the cascaded cycle could achieve larger net electrical power output and higher cycle efficiency than the basic ORC. To improve the heat recovery capability of the system, Zhang et al.[17] developed a novel combined ejector heat pump and ORC system which could output the electrical power and thermal power simultaneously. Their investigation results showed that using the combined cycle architecture, the maximum net electrical power output and maximum heat recovery capacity of the basic ORC system were improved by 10.78% and 19.04%, respectively. Besides, Li et al.[18] developed a novel combined TFC and ORC system which could also achieve high system efficiencies and large heat recovery capacity simultaneously.

According to the above literature review, it can be seen that the ORC and OFC are two famous low-temperature heat recovery cycles, which have been investigated actively for engineering applications. However, both cycles have difficulty in achieving high cycle efficiencies due to the large exergy loss of the evaporation process or throttling process. To solve this problem, many methods have been proposed, including the use of the supercritical cycle, zeotropic mixtures, two-phase expander, ejector, regenerator, multi-stage cycle, and combined cycle. Among these methods, the multi-stage (or multi-loop) cycle is a promising solution for improving the system's heat recovery capacity and efficiencies simultaneously. However, most existing studies regarding the multi-stage cycle are focused on the dual or multi-loop ORC or OFC, while the research on the mixed ORC and OFC are seldomly reported. Thus, there is a lack of information about the thermo-economic characteristics and applicable working fluids of the mixed ORC and OFC system. Moreover, it is found that the research on the performance comparison of the basic cycle and the mixed cycle is also insufficient.

To fill the above research gaps, a novel organic flash Rankine cycle (OFRC) system is investigated in this paper, based on 3E (Energy, Exergy, and Economic) analysis method and particle swarm optimization (PSO) algorithm. Five environmentally friendly organic fluids and three typical heat source conditions are simultaneously discussed in the parametric analysis and optimization process, to obtain a comprehensive understanding of the thermo-economic characteristics of this novel system. Lastly, the performance comparison of the ORC, OFC, and OFRC is performed. Overall, this paper enriches the existing research on the mixed ORC and OFC, and the obtained results provide engineers with some important hints to guide the efficient operation of the system.

2 | SYSTEMS DESCRIPTION AND WORKING FLUIDS SELECTION

2.1 | Systems description

Figure 1 presents the schematic cycle configurations of the basic ORC and OFC systems. As shown in Figure 1A, the condensed liquid (state-point 1) is pumped to the evaporator (state-point 2) where it absorbs heat from the hot fluid at constant pressure and eventually turns into the saturated or superheated vapor (state-point 3). Next, the generated vapor is introduced into a gas expander and the mechanical power is outputted during the vapor expansion process. Thereafter, the expander exhaust with a low temperature and pressure (state-point 4) is sent to the condenser where it is completely condensed into the liquid (state-point 1) to restart the cycle.

Different from the heat recovery process in the ORC system, in the OFC system, the pressurized liquid (state-point 2) is isobarically heated to be the saturated liquid (state-point 3) in the heater, avoiding the undesired

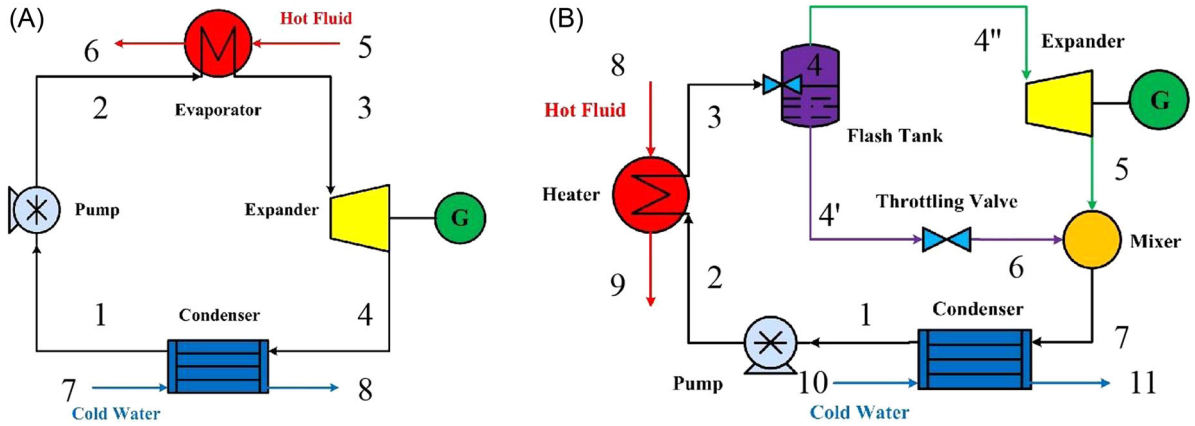

FIGURE 1 Schematic cycle configurations of (A) the basic ORC system and (B) the basic OFC system. OFC, organic flash cycle; ORC, organic Rankine cycle.

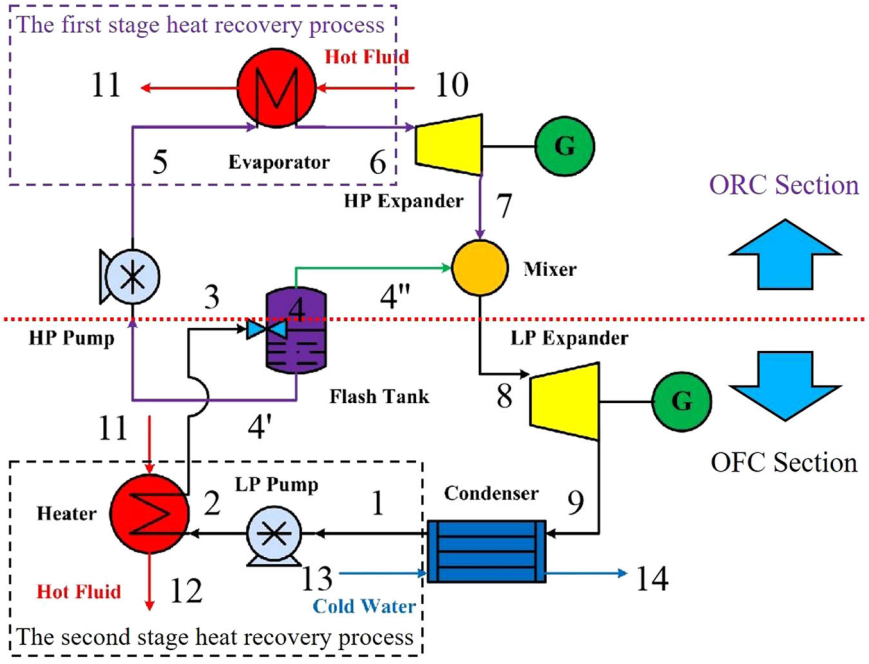

FIGURE 2 Schematic cycle configuration of the OFRC system. OFRC, organic flash Rankine cycle.

evaporating process and reducing the exergy loss of the heat recovery process. Next, the saturated liquid is throttled and is flashed into a two-phase mixture (state-point 4) in the flash tank, as illustrated in Figure 1B. The flashed vapor (state-point 4″) is introduced into a conventional gas expander to generate the mechanical power, while the bottom liquid (state-point 4′) is throttled again and then mixes with the expander exhaust (state-point 5) in the mixer. The mixture (state-point 7) is finally sent to the condenser where it is completely condensed into the liquid (state-point 1) to close the cycle. Although the basic OFC system can achieve a better heat recovery process than the basic ORC system, the two additional throttling processes cause a great exergy loss.

Figure 2 presents the schematic cycle configuration of the OFRC system. As shown in Figure 2, the OFRC system adopts a unique two-stage heat recovery process that is completed in the ORC evaporator and OFC heater. In this system, the bottom liquid (state-point 4′) of the flash tank is pressurized by the high-pressure (HP) pump without undergoing the second throttling process in the basic OFC system, while the flashed vapor (state-point 4″) is first mixed with the HP expander exhaust (state-point 7) and then enters the low-pressure (LP) expander, as depicted in Figure 2. Clearly, this novel OFRC system is a two-stage system that consists of the HP ORC stage and the LP OFC stage. Figure 3 shows the schematic temperature-specific entropy (*T*-*s*) diagram of this OFRC system.

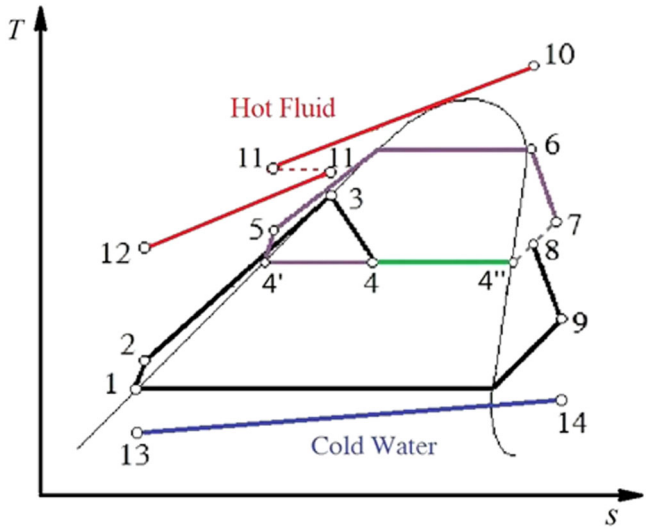

FIGURE 3 Schematic temperature-specific entropy (*T-s*) diagram of the OFRC system. OFRC, organic flash Rankine cycle.

TABLE 1 The key thermodynamic properties of the five organic fluids.

Organic fluids	T_{cr} (°C)	P_{cr} (kPa)	ODP	GWP
R601a	187.2	3378	0	20
R245fa	154.0	3651	0	1030
R600	152.0	3796	0	4
R152a	113.3	4516.8	0	124
R290	96.7	4251.2	0	3.3

Abbreviations: GWP, global warming potential; ODP, ozone depletion potential.

2.2 | Working fluids selection

Selection of the working fluid is a key step for operating a low-temperature heat recovery system because the system performance is greatly affected by the thermophysical properties of the used working fluid.[35] Li et al.[36] proposed a novel partial evaporating dual-pressure ORC system for low-grade heat recovery, and eight potential organic fluids including R290, R227ea, R152a, R124, R142b, R600, R245fa, and R601a were investigated in their paper. Since R124 is harmful to the ozone layer and both R227ea and R142b have very high global warming potential (GWP) values, these three fluids are not considered in this paper. Accordingly, the left five environmentally friendly organic fluids are selected as the potential working fluids for the OFRC system. The key thermodynamic properties and *T-s* saturation curves of these five organic fluids are presented in Table 1 and Figure 4, respectively. From Table 1 and Figure 4 it can be seen that the critical temperatures (T_{cr}) of the five organic fluids completely cover the temperature range of the low-temperature heat source in this paper (i.e., 100–140°C, see Section 4.2).

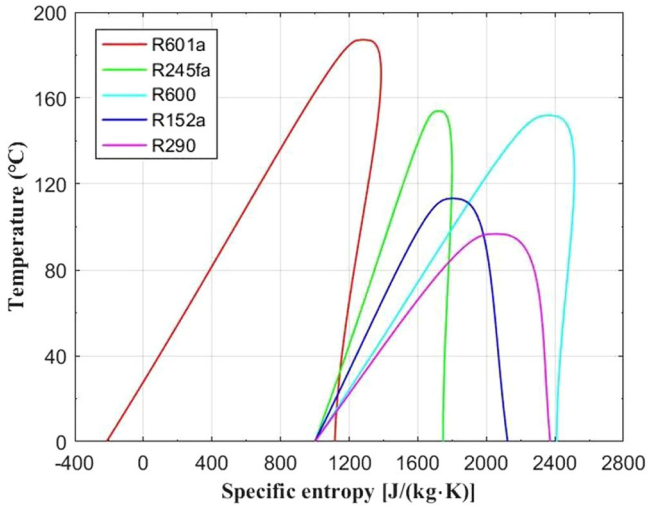

FIGURE 4 The *T-s* saturation curves of the five organic fluids.

TABLE 2 Main system parameters used in the simulation process.

Parameters (unit)	Value	Refs.
Ambient temperature (°C)	20	[13,14]
Ambient pressure (kPa)	101.325	[13,14]
Minimum heat transfer temperature difference (°C)	8	[16,37]
Temperature rise of the cooling water (°C)	10	[38]
Isentropic efficiency of expanders, $\eta_{is,exp}$ (%)	75	[13,39]
Isentropic efficiency of pumps, $\eta_{is,p}$ (%)	70	[16,39]

3 | METHODOLOGY

3.1 | Mathematical models

The main system parameters used in the simulation process are summarized in Table 2. To make the heat transfer process proceed smoothly, the minimum heat transfer temperature difference in the heat recovery unit (i.e., heater and evaporator), ΔT_{min}, is set to 8°C. In addition, several common system assumptions are adopted in this study to simplify the modeling process,[13,28] as follows:

- The system reaches the steady state.
- Changes in kinetic and potential energies of all working fluids are not considered.

- Pressure drops in all heat exchangers and pipelines are neglected.
- Heat losses of components and pipelines are negligible.
- The fluid at the evaporator outlet is saturated vapor.
- The fluid at the condenser outlet is saturated liquid.

3.1.1 | Energy model

Each component in the OFRC system can be viewed as an independent open control volume, and its mass and energy conservation equations can be respectively expressed by

$$\sum \dot{m}_{in} = \sum \dot{m}_{out}, \tag{1}$$

$$Q_{cv} = \sum (\dot{m}h)_{out} - \sum (\dot{m}h)_{in} + W_{cv}, \tag{2}$$

where Q_{cv} and W_{cv} represent the heat exchange rate and power exchange of the control volume, respectively.

For pumps and expanders, their isentropic efficiencies ($\eta_{is,p}$ and $\eta_{is,exp}$) are, respectively, calculated by

$$\eta_{is,p} = \frac{h_{is,out,p} - h_{in,p}}{h_{out,p} - h_{in,p}}, \tag{3}$$

$$\eta_{is,exp} = \frac{h_{in,exp} - h_{out,exp}}{h_{in,exp} - h_{is,out,exp}}. \tag{4}$$

As a mass ratio of the vapor mass to the total vapor–liquid mass, the vapor quality in the flash tank, x, can be calculated by

$$x = \frac{\dot{m}_{4''}}{\dot{m}_4} = \frac{h_4 - h_{4'}}{h_{4''} - h_{4'}}. \tag{5}$$

The detailed mass and energy conservation equations of each component in the OFRC system are shown in Table 3.

Thus, the net power output of the system, W_{net}, can be calculated by

$$\begin{aligned} W_{net} &= (W_{exp,HP} + W_{exp,LP}) \cdot \eta_m \cdot \eta_G - W_{p,HP} \\ &\quad - W_{p,LP} - W_{cp} \\ &= (W_{exp,HP} + W_{exp,LP}) \cdot \eta_m \cdot \eta_G - W_{p,HP} \\ &\quad - W_{p,LP} - \frac{\dot{m}_{cw} g H \times 10^{-3}}{\eta_{cp}}, \end{aligned} \tag{6}$$

where η_m, η_G, and η_{cp} are the mechanical efficiency, generator efficiency and circulating pump efficiency, which are set to 0.97, 0.98 and 0.80,[33] respectively. W_{cp} and $\dot{m}_{cw}$ are the power consumption of the circulating pump in the cooling system and the mass flow rate of the cooling water, respectively. Besides this, g is the gravitational acceleration ($9.8\ \mathrm{m\ s^{-2}}$) and H is the circulating pump head (set to 20 m[40]).

Since most low-temperature heat sources will be discarded after being used, the global thermal efficiency ($\eta_{th,g}$) counting the unrecovered thermal energy (or the wasted thermal energy) is adopted in this study to evaluate the overall thermodynamic performance of the system, as follows:

TABLE 3 Mass and energy conservation equations of each component in the OFRC system.

Components	Mass balance equations	Energy balance equations
LP pump	$\dot{m}_1 = \dot{m}_2$	$W_{p,LP} = \dot{m}_1(h_2 - h_1) = \frac{\dot{m}_1(h_{is,2} - h_1)}{\eta_{is,p}}$
Heater	$\dot{m}_2 = \dot{m}_3$, $\dot{m}_{11} = \dot{m}_{12}$	$Q_{heater} = \dot{m}_2(h_3 - h_2) = \dot{m}_{11}(h_{11} - h_{12})$
Flash tank	$\dot{m}_3 = \dot{m}_4 = \dot{m}_{4'} + \dot{m}_{4''}$	$\dot{m}_3 h_3 = \dot{m}_4 h_4 = \dot{m}_{4'} h_{4'} + \dot{m}_{4''} h_{4''}$
HP pump	$\dot{m}_{4'} = \dot{m}_5$	$W_{p,HP} = \dot{m}_{4'}(h_5 - h_{4'}) = \frac{\dot{m}_{4'}(h_{is,5} - h_{4'})}{\eta_{is,p}}$
Evaporator	$\dot{m}_5 = \dot{m}_6$, $\dot{m}_{10} = \dot{m}_{11}$	$Q_{eva} = \dot{m}_5(h_6 - h_5) = \dot{m}_{10}(h_{10} - h_{11})$
HP expander	$\dot{m}_6 = \dot{m}_7$	$W_{exp,HP} = \dot{m}_6(h_6 - h_7) = \dot{m}_6(h_6 - h_{is,7}) \cdot \eta_{is,exp}$
Mixer	$\dot{m}_7 + \dot{m}_{4''} = \dot{m}_8$	$\dot{m}_7 h_7 + \dot{m}_{4''} h_{4''} = \dot{m}_8 h_8$
LP expander	$\dot{m}_8 = \dot{m}_9$	$W_{exp,LP} = \dot{m}_8(h_8 - h_9) = \dot{m}_8(h_8 - h_{is,9}) \cdot \eta_{is,exp}$
Condenser	$\dot{m}_9 = \dot{m}_1$, $\dot{m}_{13} = \dot{m}_{14}$	$Q_{con} = \dot{m}_9(h_9 - h_1) = \dot{m}_{13}(h_{14} - h_{13})$

Abbreviation: OFRC, organic flash Rankine cycle.

$$\eta_{th,g} = \frac{W_{net}}{Q_{rec,tot}} = \frac{Q_{eva} + Q_{heater}}{Q_{rec,tot}} \cdot \frac{W_{net}}{Q_{eva} + Q_{heater}} = \alpha \cdot \eta_{th}, \quad (7)$$

where $Q_{rec,\ tot}$ represents the total recyclable heat and can be calculated by Equation (8). Q_{eva} and Q_{heater} are the heat exchange rates of the evaporator and heater (see Table 3), respectively. α and η_{th} denote the heat recovery ratio (reflecting the system's heat recovery capability) and the cycle thermal efficiency (representing the effective utilization degree of the recovered heat), respectively.

$$Q_{rec,tot} = \dot{m}_{hs}(h_{in,hs} - h_0) = \dot{m}_{10}(h_{10} - h_0), \quad (8)$$

where subscripts *hs* and 0 represent the heat source and ambient conditions, respectively.

3.1.2 | Exergy model

The exergy conservation equation of each component in the OFRC system can be expressed as

$$Ex_{Q_{cv}} = \sum(\dot{m} \cdot ex)_{out} - \sum(\dot{m} \cdot ex)_{in} + W_{cv} + I_{cv}, \quad (9)$$

where *Ex* and *I* represent the exergy flow rate and exergy loss rate, respectively.

In this study, only physical exergy is taken into consideration while other exergies such as kinetic exergy, potential exergy, and chemical exergy are not considered.[13] Thus, the specific exergy at state-point *i* can be calculated by

$$ex_i = h_i - h_0 - (T_0 + 273.15) \cdot (s_i - s_0). \quad (10)$$

The detailed exergy balance and exergy efficiency equations of each component in the OFRC system are presented in Table 4.

Thus, the total exergy loss (I_{tot}) and global exergy efficiency ($\eta_{exg,g}$) of the OFRC system can be respectively calculated by

$$I_{tot} = Ex_{rec,tot} - W_{net} = Ex_{10} - W_{net}, \quad (11)$$

$$\eta_{exg,g} = \frac{W_{net}}{Ex_{rec,tot}} = \frac{Ex_{10} - Ex_{12}}{Ex_{10}} \cdot \frac{W_{net}}{Ex_{10} - Ex_{12}} = \beta \cdot \eta_{exg}, \quad (12)$$

where Ex_{10} and Ex_{12} are the exergy flow rates at state-points 10 and 12 (i.e., the total recyclable exergy ($Ex_{rec,tot}$) and the unrecovered exergy), respectively. β and η_{exg} represent the exergy recovery ratio and the cycle exergy efficiency, respectively.

3.1.3 | Economic model

The system's economic cost is also an important performance index, especially for some small or micro-scale systems.[41] To obtain some preliminary estimation results about the economic performance difference of the ORC, OFC, and OFRC, the cost function method is used to roughly calculate the investment cost of the system. Therefore, the total investment cost of the system, C_{tot}, can be calculated by

TABLE 4 Exergy balance and exergy efficiency equations of each component in the OFRC system.

Components	Exergy balance equations	Exergy efficiency equations
LP pump	$I_{p,LP} = Ex_1 + W_{p,LP} - Ex_2$	$\eta_{exg,p,LP} = \frac{Ex_2 - Ex_1}{W_{p,LP}}$
Heater	$I_{heater} = Ex_2 + Ex_{11} - Ex_3 - Ex_{12}$	$\eta_{exg,heater} = \frac{Ex_3 - Ex_2}{Ex_{11} - Ex_{12}}$
Flash tank	$I_{ft} = Ex_3 - Ex_{4'} - Ex_{4''}$	$\eta_{exg,ft} = \frac{Ex_{4'} + Ex_{4''}}{Ex_3}$
HP pump	$I_{p,HP} = Ex_{4'} + W_{p,HP} - Ex_5$	$\eta_{exg,p,HP} = \frac{Ex_5 - Ex_{4'}}{W_{p,HP}}$
Evaporator	$I_{eva} = Ex_5 + Ex_{10} - Ex_6 - Ex_{11}$	$\eta_{exg,eva} = \frac{Ex_6 - Ex_5}{Ex_{10} - Ex_{11}}$
HP expander	$I_{exp,HP} = Ex_6 - Ex_7 - W_{exp,HP}$	$\eta_{exg,exp,HP} = \frac{W_{exp,HP}}{Ex_6 - Ex_7}$
Mixer	$I_{mixer} = Ex_7 + Ex_{4''} - Ex_8$	$\eta_{exg,mixer} = \frac{Ex_8}{Ex_7 + Ex_{4''}}$
LP expander	$I_{exp,LP} = Ex_8 - Ex_9 - W_{exp,LP}$	$\eta_{exg,exp,LP} = \frac{W_{exp,LP}}{Ex_8 - Ex_9}$
Condenser	$I_{con} = Ex_9 - Ex_1$	$\eta_{exg,con} = 0$

Abbreviation: OFRC, organic flash Rankine cycle.

$$C_{tot} = \sum_{i=1}^{j} C_{i,ref}\left(\frac{\text{CEPCI}_{2020}}{\text{CEPCI}_{ref}}\right), \tag{13}$$

where $C_{j,ref}$ represents the ith component's investment cost based on the reference year, and CEPCI denotes the Chemical Engineering Plant Cost Index.

The detailed investment cost models of each component in the OFRC system are shown in Table 5. In this study, the condenser is considered as the shell and tube heat exchanger while the heater and evaporator are treated as the compact heat exchanger. Their investment costs are preliminarily estimated based on the size of the heat transfer area which can be calculated using the logarithmic mean temperature difference (LMTD) method.[42,43] In addition, the investment costs of other components such as flash tank and mixer are omitted because of their small values.[28,42]

Thus, the system's total investment cost rate, c_{tot}, can be calculated by considering the capital recovery factor (CRF) and annual operating hours (N), shown as

$$c_{tot} = \frac{C_{tot}\,\text{CRF}}{N}, \tag{14}$$

$$\text{CRF} = \frac{j(1+j)^n}{(1+j)^n - 1}, \tag{15}$$

where the annual operating hours (N), interest rate (j) and lifetime (n) of the system are set to 8000 h, 12% and 20 years,[42,43] respectively.

In addition to the equipment investment cost, the fuel cost and operation and maintenance cost should also be counted in the modeling process. Since the heat source in this paper is the low-temperature waste heat, the fuel cost is neglected. The system's operation and maintenance cost rate, c_{OM}, can be calculated by

$$c_{OM} = \frac{\gamma \cdot C_{tot}}{N}, \tag{16}$$

where the maintenance factor (γ) is set to 0.06.[42,43]

Thus, the system's specific power cost or levelized cost of electricity (LCOE, $\$\,\text{kW}^{-1}\,\text{h}^{-1}$) can be calculated by

$$\text{LCOE} = \frac{c_{tot} + c_{OM}}{W_{net}}. \tag{17}$$

3.2 | Optimization

Conducting the system optimization is very necessary and important for the operation of a low-temperature heat recovery system because the system's thermo-economic performance could be greatly affected by several key operating parameters. In this study, the PSO algorithm of the MATLAB optimization toolbox is invoked to search the optimal operating conditions of the system, and its calculation flowchart is presented in Figure 5.

It is seen that after the initialization of the PSO algorithm, particles are assigned to the selected optimization variables, and then, all state-point parameters of the system are calculated based on the mathematical models given in the previous section. Next, the PSO analysis is conducted and the PSO fitness value is evaluated to update the best solutions (for individual particles and the entire particle swarm) and check whether the convergence criteria have been satisfied. If so, the PSO calculation will be completed and the best solution will be obtained and outputted. If not, the position and velocity (X & v) vectors of the particle will be updated according to the following equations:

TABLE 5 Investment cost models of each component in the OFRC system.

Components	Investment cost models	Reference year	Refs.
Condenser	$C_{con} = 2143 \cdot A_{con}^{0.514}$ $A_{con} = \frac{Q_{con}}{U_{con} \cdot \Delta T_{LMTD,con}}$ $U_{con} = 2.0\ \text{kW/m}^2\cdot\text{K}$	1986	[42,43]
Heater	$C_{heater} = 2681 \cdot A_{heater}^{0.59}$ $A_{heater} = \frac{Q_{heater}}{U_{heater} \cdot \Delta T_{LMTD,heater}}$ $U_{heater} = 1.6\ \text{kW/m}^2\cdot\text{K}$	1986	[42]
Evaporator	$C_{eva} = 2681 \cdot A_{eva}^{0.59}$ $A_{eva} = \frac{Q_{eva}}{U_{eva} \cdot \Delta T_{LMTD,eva}}$ $U_{eva} = 1.6\ \text{kW/m}^2\cdot\text{K}$	1986	[43]
Expanders	$C_{exp,LP} = 4405 \cdot W_{exp,LP}^{0.7}$ $C_{exp,HP} = 4405 \cdot W_{exp,HP}^{0.7}$	2005	[42,43]
Pumps	$C_{p,LP} = 1120 \cdot W_{p,LP}^{0.8}$ $C_{p,HP} = 1120 \cdot W_{p,HP}^{0.8}$ $C_{cp} = 1120 \cdot W_{cp}^{0.8}$	2005	[42,43]
Generator[a]	$C_G = 60 \cdot (W_{exp,LP} + W_{exp,HP})^{0.95}$	2005	[44]

Abbreviation: OFRC, organic flash Rankine cycle.

[a]Only one generator is used in the OFRC system, which means that the HP expander and the LP expander are coaxial.

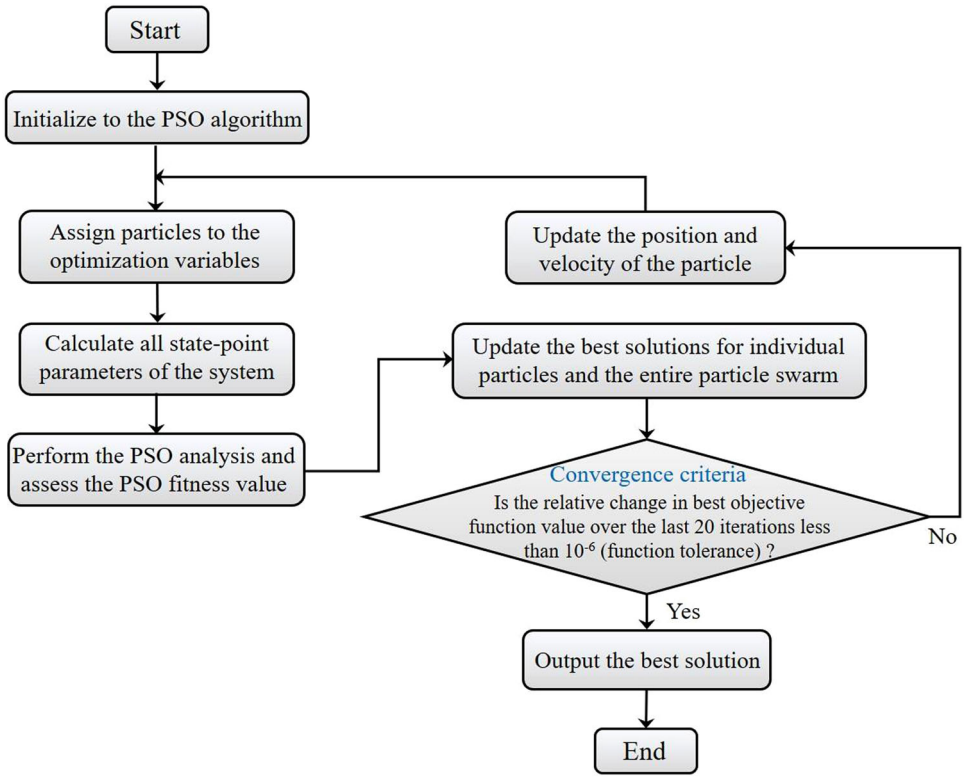

FIGURE 5 Calculation flowchart of the PSO algorithm. PSO, particle swarm optimization.

$$X_{ij}^{k+1} = X_{ij}^{k} + v_{ij}^{k+1}, \tag{18}$$

$$v_{ij}^{k+1} = wv_{ij}^{k} + a_1 Rand_1\left(X_{pb,ij}^{k} - X_{ij}^{k}\right) + a_2 Rand_2\left(X_{gb,ij}^{k} - X_{ij}^{k}\right), \tag{19}$$

where the superscript k represents the current number of iterations; the subscripts i and j denote the positive integers indexing the particle and the dimension of the solution space (or the number of the optimization variables), respectively; the term w is the inertia weight that balances the local and global search capabilities of the algorithm; the symbols a and $Rand$ represent the acceleration coefficient and random number, respectively; the subscripts pb and gb denote the personal best and global best, respectively.

3.3 | Model validation

The MATLAB/Simulink software[45] assisted with the NIST REFPROP database[46] is used to construct the above mathematical models, and the simulation results are validated by referring to the relevant published literature. Since the OFRC system essentially consists of two basic systems (i.e., ORC and OFC), the model verification can be completed by validating the simulation results of the two basic systems, as shown in Table 6.

It can be seen from Table 6 that the simulation results of this paper are consistent with the results reported in Refs. [42,43], which means that the mathematical models and solving procedures developed in the MATLAB software are reliable for the subsequent analysis.

4 | RESULTS AND DISCUSSION

4.1 | Simulation results

It is assumed that the low-temperature heat source in this paper is the liquid water (such as the geothermal water or industrial wastewater) that has a constant mass flow rate of 89 kg/s, a specified pressure of 700 kPa, and a rated inlet temperature of 122°C.[47] Table 7 lists the rated operating parameters of the OFRC system under this heat source condition.

Under the rated operating condition, the system performance results are presented in Figure 6 and the detailed system state-point parameters are summarized in Table 8. From Figure 6A,B it can be seen that under the rated operating condition, the OFRC system can achieve a net electrical power output of 1105.5 kW, a global thermal efficiency of 2.9%, and a global exergy efficiency of 20.2%. About half of the total recyclable heat ($Q_{rec,tot}$) and about 30% of the total recyclable exergy

TABLE 6 Model validation of the basic (A) ORC system[a] and (B) OFC system.[b]

(A) ORC system									
	P (kPa)			*T* (°C)			*h* (kJ/kg)		
State-points	Ref. [43]	This study	Error (%)	Ref. [43]	This study	Error (%)	Ref. [43]	This study	Error (%)
1	110	110	0	30	30	0	230.26	230.26	0
2	624	624	0	30.27	30.27	0	230.70	230.70	0
3	624	624	0	90	90	0	434.43	434.43	0
4	110	110	0	44.32	44.32	0	409.70	409.70	0
7	101	101	0	25	25	0	104.92	104.92	0
8	101	101	0	27.12	27.12	0	113.78	113.78	0
(B) OFC system									
	P (kPa)			*T* (°C)			*h* (kJ/kg)		
State-points	Ref. [42]	This study	Error (%)	Ref. [42]	This study	Error (%)	Ref. [42]	This study	Error (%)
1	250	250	0	40	40	0	252.57	252.57	0
2	1549	1549	0	40.70	40.70	0	253.82	253.82	0
3	1549	1549	0	109.36	109.36	0	354.80	354.80	0
4	789	789	0	80	80	0	354.80	354.80	0
4′	789	789	0	80	80	0	309.24	309.24	0
4″	789	789	0	80	80	0	461.75	461.75	0
5	250	250	0	51.18	51.18	0	444.95	444.95	0
6	250	250	0	40	40	0	309.24	309.24	0
7	250	250	0	40	40	0	349.78	349.78	0
10	101	101	0	25	25	0	104.92	104.92	0
11	101	101	0	30	30	0	125.82	125.82	0

Abbreviations: OFC, organic flash cycle; ORC, organic Rankine cycle.

[a] $T_0 = 25°C$, $T_{con} = 30°C$, $T_{eva} = 90°C$, $\Delta T_{sup} = 0°C$, $\Delta T_{pp,con} = 3°C$, $\eta_{is,exp} = 0.85$, $\eta_{is,p} = 0.80$, working fluid: R123.

[b] $T_0 = 25°C$, $T_{con} = 40°C$, $T_3 = 109.36°C$, $T_4 = 80°C$, $\Delta T_{pp,con} = 10°C$, $\eta_{is,exp} = 0.80$, $\eta_{is,p} = 0.80$, working fluid: R245fa.

TABLE 7 The OFRC system's rated operating parameters.

Parameters (unit)	Value
Working fluid	R152a[a]
Evaporation temperature, T_{eva} (°C)	85
Outlet temperature of the heater, T_3 (°C)	75
Flashing temperature, T_4 (°C)	65
Condensation temperature, T_{con} (°C)	40

Abbreviation: OFRC, organic flash Rankine cycle.

[a] Its critical temperature (113.3°C) is close to the heat source inlet temperature (122°C).

($Ex_{rec,tot}$) are not recovered and are directly dumped to the environment. According to the exergy loss distribution shown in Figure 6C, the system's biggest exergy loss (about 41.7% of the total exergy loss) is caused by the condenser where a large amount of low-temperature heat is released to the environmental cooling water (thus, the exergy efficiency of condenser is equal to 0). The system's second biggest exergy loss (about 23.5% of the total exergy loss) is occupied by the evaporator which has a moderate exergy efficiency of approximately 80%, as illustrated in Figure 6C. In general, the main exergy loss sources of the OFRC system come from the condenser and evaporator as more than 60% of the total exergy loss is caused by these two components.

The economic analysis results show that under the rated operating condition, the OFRC system can achieve a specific power cost of 0.0398 $/(kW·h), and about 70% and 30% of the specific power cost are caused by the total capital investment cost and the operation and maintenance cost, respectively. Besides, among all system components, the LP expander and the HP expander are the two most expensive components, whose investment cost accounts for about 63.7% of the total investment cost, as shown in Figure 6D.

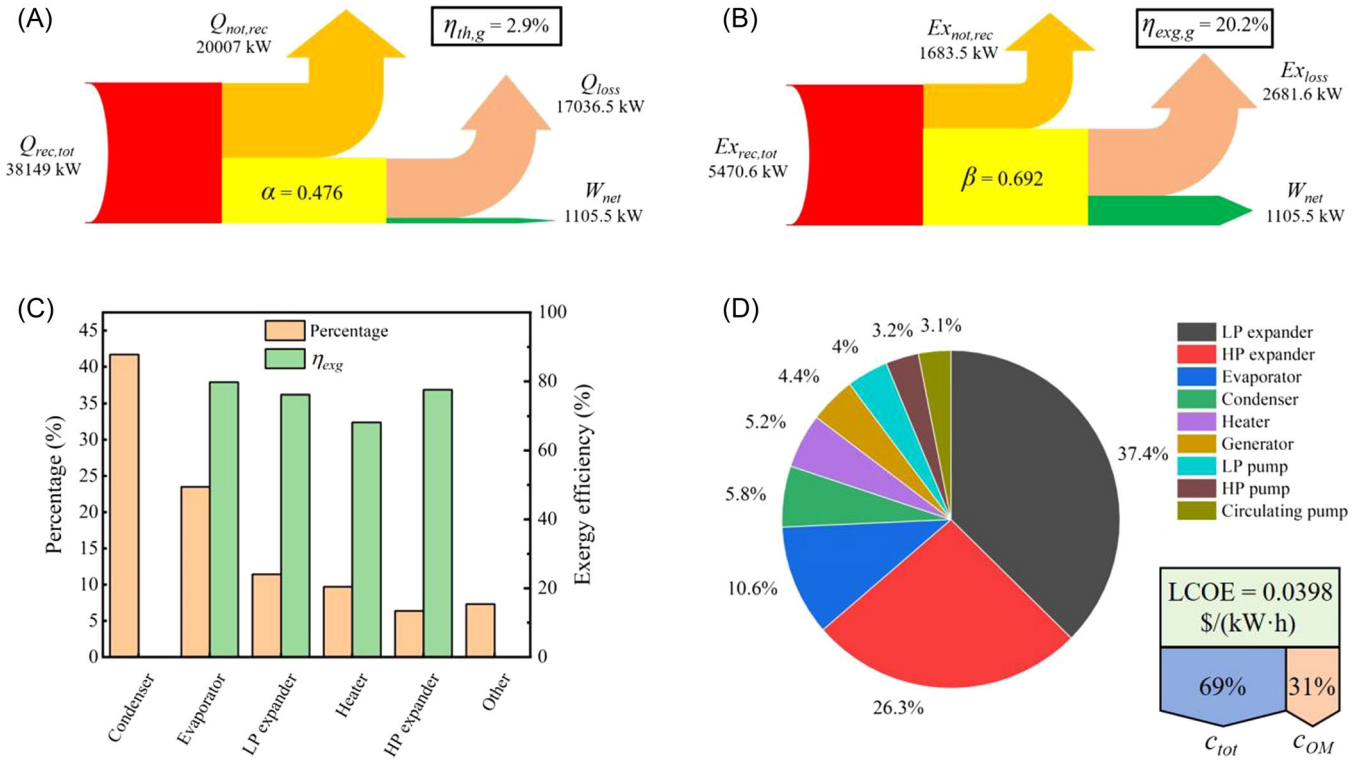

FIGURE 6 Performance results of the OFRC system under the rated operating condition: (A) energy flow diagram, (B) exergy flow diagram, (C) exergy loss distribution, and (D) investment cost distribution. OFRC, organic flash Rankine cycle.

TABLE 8 The detailed state-point parameters of the OFRC system under the rated operating condition.

State-points	Fluids	$\dot{m}$ (kg/s)	T (°C)	P (kPa)	h (kJ/kg)	s (kJ/kg·K)
1	R152a	67.67	40	909.3	271.35	1.241
2	R152a	67.67	41.09	2105.1	273.33	1.243
3	R152a	67.67	75	2105.1	341.98	1.450
4	R152a	67.67	65	1685.3	341.98	1.453
4′	R152a	61.12	65	1685.3	320.64	1.390
4″	R152a	6.55	65	1685.3	541.21	2.042
5	R152a	61.12	66.13	2599.6	322.31	1.391
6	R152a	61.12	85	2599.6	543.13	2.011
7	R152a	61.12	65	1685.3	533.80	2.020
8	R152a	67.67	65	1685.3	534.52	2.022
9	R152a	67.67	40	909.3	520.55	2.037
10	Water	89	122	700	512.65	1.549
11	Water	89	86.07	700	361.00	1.147
12	Water	89	73.63	700	308.81	0.999
13	Water	403.27	20	101.3	84.01	0.297
14	Water	403.27	30	101.3	125.82	0.437

Abbreviation: OFRC, organic flash Rankine cycle.

4.2 | Parametric analysis

In the actual operation process, the heat source condition is usually unstable and always fluctuates within a certain range. In this paper, the inlet temperature of the heat source, $T_{in,hs}$, is set to vary in the temperature range of 100–140°C which is determined based on a possible temperature fluctuation of about 20°C (with regard to the rated value of 122°C). Therefore, three typical cases considering different heat source inlet temperatures are analyzed comparatively in this section, which is presented in Table 9. It is not difficult to find that there are three key operating parameters that may have great effects on the thermo-economic performance of the OFRC system, which are the evaporation temperature (or evaporation pressure), the heater outlet temperature (or heating pressure), and the flashing temperature (or flashing pressure), respectively. Thus, for different cases, the rated values of these three parameters are considered to be different (see Table 9). However, it should be emphasized that for each case, the method of controlling variable is used, which means that the other operating parameters are kept unchanged when investigating the effects of one operating parameter on the system performance.

4.2.1 | Effects of the evaporation temperature on the system performance

Figure 7 shows the effects of the evaporation temperature (T_{eva}) on the system performance. As shown in Section 3.1, there are four different performance indexes that have been calculated to evaluate the performance of the OFRC system, which are the net electrical power output (W_{net}), global thermal efficiency ($\eta_{th,g}$), global exergy efficiency ($\eta_{exg,g}$), and specific power cost (LCOE), respectively. According to Equations (7) and (12), both the global thermal and exergy efficiencies exclusively depend on the value of the net electrical power output, because under a determined heat source condition, the denominators of Equations (7) and (12) (namely, the total recyclable heat, $Q_{rec,tot}$, and the total recyclable exergy, $Ex_{rec,tot}$) are two constants. Thus, it can be inferred that the global thermal and exergy efficiencies have a similar evolution process to the net electrical power output, which means that we only need to investigate the changes in the net electrical power output and specific power cost at this time.

From Figure 7(A1), (B1), and (C1) it can be seen that for all cases and working fluids, as the evaporation temperature increases, the system's net electrical power output first increases and then decreases significantly, while the specific power cost first decreases slightly and then increases rapidly. Thus, it can be speculated that there is an optimal evaporation temperature that makes the OFRC system achieve the best thermo-economic performance (the value of this optimal evaporation temperature varies with the heat source condition). Here we take the R290 in Case I as an example. When the evaporation temperature (T_{eva}) increases from 65°C to 90°C, the system's net electrical power output first increases from about 453 to 492 kW and then decreases rapidly to about 99 kW. At the same time, the specific power cost first decreases slightly from about 0.062 \$/(kW·h) to 0.060 \$/(kW·h) and then increases dramatically to about 0.101 \$/(kW·h). It is found that when the evaporation temperature is equal to about 70°C, the OFRC system can achieve the best thermo-economic performance.

According to Equation (7), the system's global thermal efficiency is equal to the product of the heat recovery ratio (α, reflecting the system's heat recovery capability) and the cycle thermal efficiency (η_{th}, representing the effective utilization degree of the recovered heat). Thus, the change in the net electrical power output can be explained by analyzing these two parameters, as presented in Figure 7(A2), (B2), and (C2). From these figures, it can be clearly seen that the cycle thermal efficiency increases gradually with the increase of the evaporation temperature, while the heat recovery ratio first remains almost unchanged (or has a tiny decrease) and then drops approximately linearly. Since the value of the heat recovery ratio directly reflects the amount of the recovered heat (i.e., the heat input to the system), the above evolution process of the net electrical power output is eventually caused.

TABLE 9 The system's rated operating parameters under three typical cases.

Parameters (unit)	Case I	Case II	Case III
Inlet temperature of the heat source, $T_{in,hs}$ (°C)	100	120	140
Evaporation temperature, T_{eva} (°C)	70	85	100
Outlet temperature of the heater, T_3 (°C)	65	75	85
Flashing temperature, T_4 (°C)	60	65	70
Condensation temperature, T_{con} (°C)	40	40	40

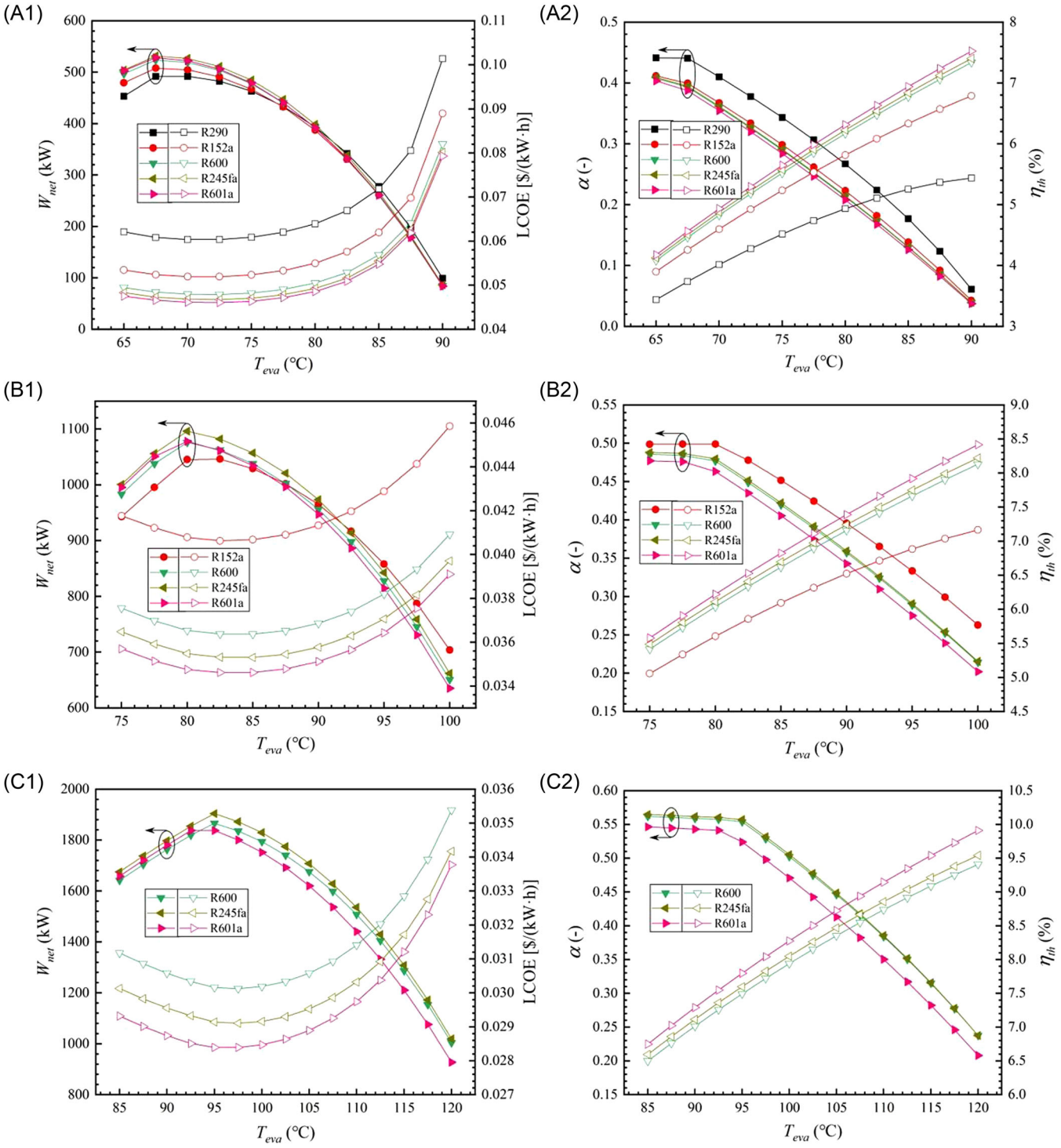

FIGURE 7 Effects of the evaporation temperature on the system performance: (A) Case I, (B) Case II, and (C) Case III.

In addition, it should be noted that for Cases II and III, not all five working fluids are discussed when analyzing the effects of the evaporation temperature on the system performance (e.g., only three working fluids are investigated in Case III). This is because the highest evaporation temperatures in these two cases exceed the critical temperatures (T_{cr}) of several organic fluids (e.g., in Case III, the highest evaporation temperature is equal to 120°C that is higher than the critical temperatures of R290 and R152a). To avoid the over-high operating pressures of the supercritical conditions and the unstable fluid thermophysical properties of the trans-critical conditions, in this study, the OFRC system is limited to operate at the stable and safe subcritical conditions.

4.2.2 | Effects of the heater outlet temperature on the system performance

Figure 8 shows the effects of the heater outlet temperature (T_3) on the system performance. From Figure 8(A1), (B1), and (C1) it can be seen that with the increase of the heater outlet temperature, the system's net electrical power output first increases slightly and then decreases approximately linearly, while the specific power cost increases gradually and the rate of increase is also getting faster. Thus, it can be speculated that there is also an optimal heater outlet temperature that makes the OFRC system achieve the best thermo-economic performance (the value of this optimal heater outlet temperature

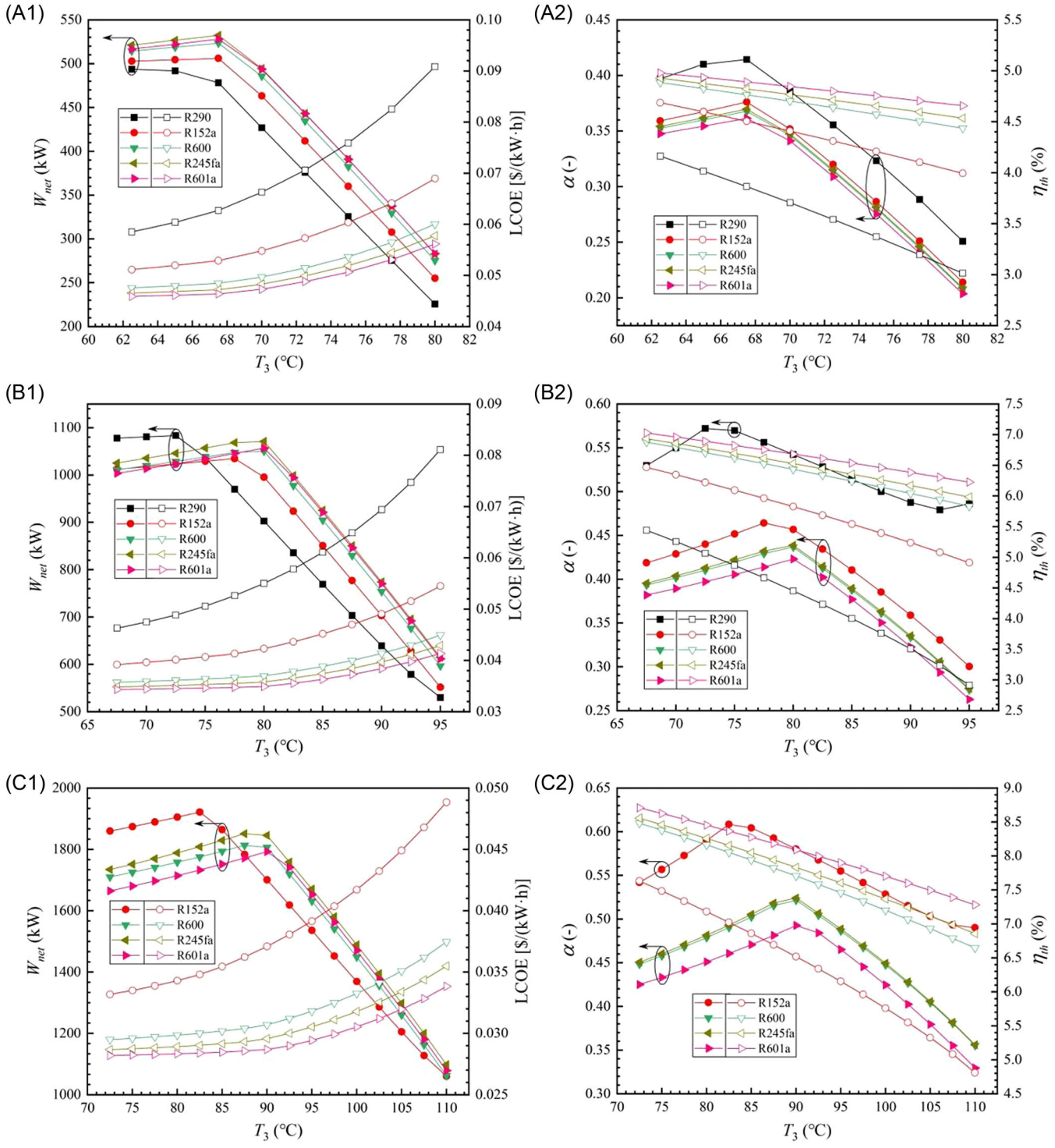

FIGURE 8 Effects of the heater outlet temperature on the system performance: (A) Case I, (B) Case II, and (C) Case III.

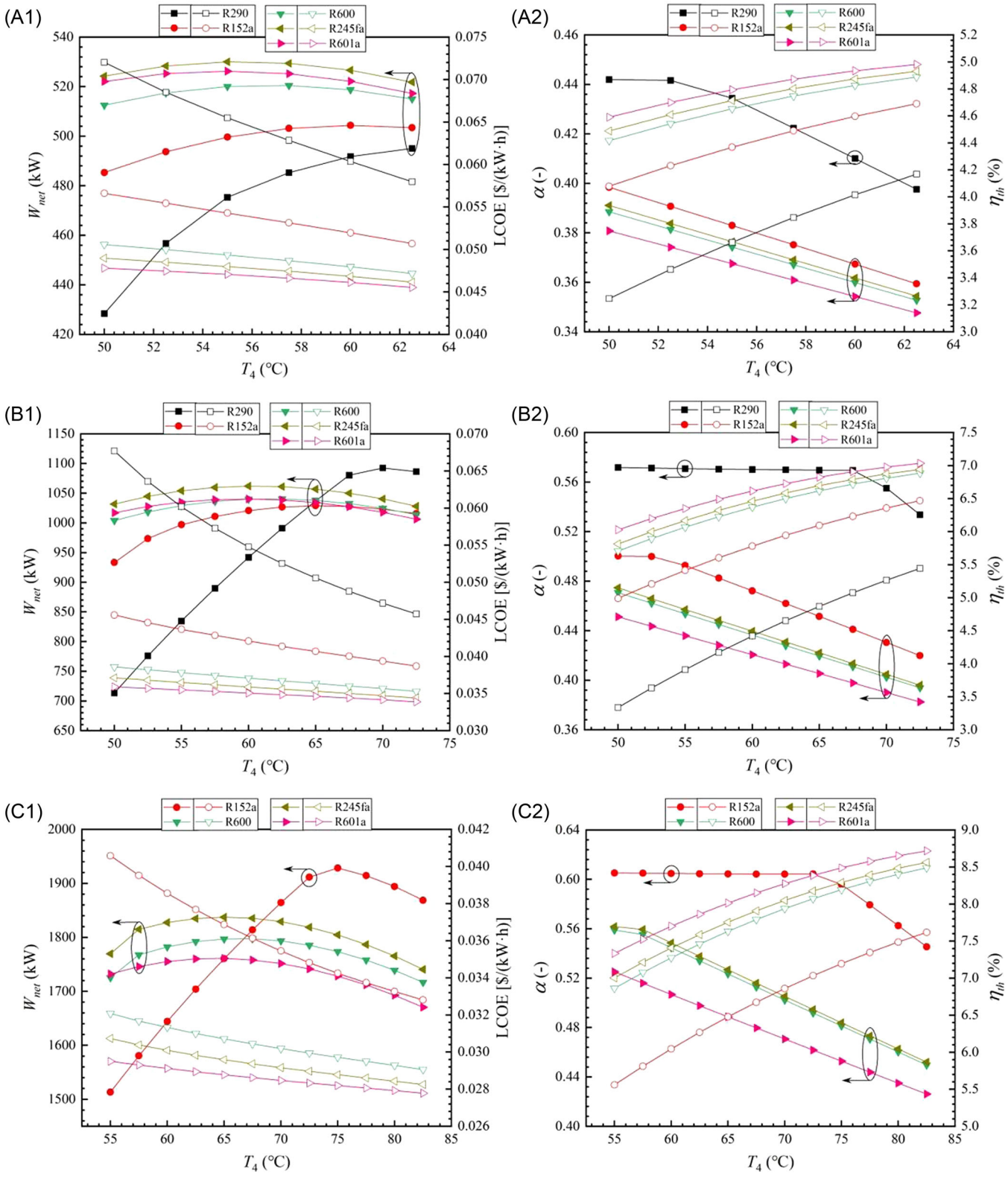

FIGURE 9 Effects of the flashing temperature on the system performance: (A) Case I, (B) Case II, and (C) Case III.

varies with the heat source condition). Here we take the R152a in Case II as an example. When the heater outlet temperature (T_3) increases from 67.5°C to 77.5°C, the system's net electrical power output increases from about 1012 to 1035 kW, and the specific power cost increases slightly from about 0.039 $/(kW·h) to 0.041 $/(kW·h). However, as the heater outlet temperature continues to increase to 95°C, the net electrical power output will

rapidly decrease to about 552 kW and the specific power cost will increase to about 0.054 $/(kW·h). Thus, it is predicted that the OFRC system can achieve the best thermo-economic performance when the heater outlet temperature is equal to around 70–75°C.

Overall, the heat recovery ratio (α) has a similar evolution process to the net electrical power output, while the cycle thermal efficiency (η_{th}) decreases approximately linearly, as illustrated in Figure 8(A2), (B2), and (C2). As discussed earlier, the amount of the recovered heat (or the heat input to the system) is directly determined by the heat recovery ratio, which means that the heat recovery ratio may have a greater impact on the system performance than the cycle thermal efficiency. Thus, the above evolution process of the net electrical power output is caused.

4.2.3 | Effects of the flashing temperature on the system performance

Figure 9 presents the effects of the flashing temperature (T_4) on the system performance. From Figure 9(A1), (B1), and (C1) it can be seen that as the flashing temperature increases, the system's net electrical power output first increases and then decreases, while the specific power cost decreases continuously. Thus, it can be concluded that there is an optimal flashing temperature that makes the OFRC system achieve the best thermodynamic performance, and increasing the flashing temperature can enhance the OFRC system's economic performance. Here we take the R600 in Case III as an example. When the flashing temperature (T_4) increases from 55°C to 82.5°C, the system's net electrical power output first increases from about 1725 to 1797 kW and then decreases to about 1717 kW, and the specific power cost decreases gradually from about 0.032 $/(kW·h) to 0.029 $/(kW·h). It is found that when the flashing temperature is equal to about 67.5°C, the OFRC system can achieve the best thermodynamic performance, and the best economic performance can be achieved when the flashing temperature is set to 82.5°C.

According to Figure 9(A2), (B2), and (C2), it can be found that with the increase of the flashing temperature, the heat recovery ratio (α) shows two different evolution processes, but the cycle thermal efficiency (η_{th}) always increases gradually. In more detail, for the working fluids with relatively low critical temperatures, as the flashing temperature increases, the heat recovery ratio first remains almost unchanged and then decreases gradually. But, for the working fluids with relatively high critical temperatures, the heat recovery ratio decreases approximately linearly with the increase of the flashing temperature. It is not difficult to find that the magnitude of the variation of the heat recovery ratio (α) in Figure 9 is significantly smaller than that in Figures 7 and 8. At this time, the effects of the cycle thermal efficiency (η_{th}) on the system performance cannot be underestimated. Therefore, the change in the net electrical power output is caused by the combined effects of the heat recovery ratio and cycle thermal efficiency at this time.

Overall, compared to the evaporation temperature and heater outlet temperature, the flashing temperature has a smaller effect on the system performance, and under the same operating conditions, the higher the critical temperature of the working fluid, the lower the specific power cost of the system (i.e., the better the economic performance of the system), as shown in Figures 7–9. Besides this, it is found that compared to the working fluids with low critical temperatures (R290 and R152a), the working fluids with high critical temperatures (R600, R245fa, and R601a) have higher cycle thermal efficiency (η_{th}), which means that they can achieve more efficient use of the heat input to the system. However, the working fluids with low critical temperatures have a larger heat recovery ratio (α), which means that they can improve the heat recovery capability of the system.

4.3 | Optimization and comparison of ORC, OFC, and OFRC

The tuning parameters of the PSO algorithm, the optimization variable settings, and several key operating

TABLE 10 PSO tuning parameters, optimization variables, and operating constraints.

Tuning parameters	**Value**
Hybrid function solver	fmincon
Swarm size	50
Maximum number of iterations	600
Function tolerance	10^{-6}
Optimization variables (Unit)	**Range**
Evaporation temperature, T_{eva} (°C)	55–150
Heater outlet temperature, T_3 (°C)	55–150
Flashing temperature, T_4 (°C)	45–140
Operating constraints (Unit)	**Value**
The maximum evaporation temperature, $T_{eva,max}$ (°C)	$\leq(T_{cr}-5)$
The maximum heater outlet temperature, $T_{3,max}$ (°C)	$\leq(T_{cr}-5)$
The vapor quality in flash tank, x	$0.1 \leq x \leq 0.9$

Abbreviation: PSO, particle swarm optimization.

TABLE 11 Optimized decision variables and the corresponding system performance results: (A) Case I ($T_{in,hs} = 100°C$), (B) Case II ($T_{in,hs} = 120°C$), and (C) Case III ($T_{in,hs} = 140°C$).

(A) Case I															
	R290			**R152a**			**R600**			**R245fa**			**R601a**		
Parameters (unit)	**ORC**	**OFC**	**OFRC**	**ORC**	**OFC**	**OFRC**	**ORC**	**OFC**	**OFRC**	**ORC**	**OFC**	**OFRC**	**ORC**	**OFC**	**OFRC**
T_{eva} (°C)	68.82	-	70.53	67.97	-	69.19	67.75	-	68.9	67.78	-	68.85	67.59	-	68.54
T_3 (°C)	-	91.7	67.08	-	92	66	-	92	65.86	-	92	65.77	-	92	65.52
T_4 (°C)	-	71.36	59.19	-	68.36	54.25	-	67.19	53.54	-	67.07	53.59	-	66.8	52.43
W_{net} (kW)	497.72	−96.69	486.56	503.29	−40.83	499.52	512.51	194.34	522.66	518.09	279.70	533.80	514.38	338.82	530.50
$\eta_{th,g}$ (%)	1.67	-	1.63	1.68	-	1.67	1.72	0.65	1.75	1.73	0.94	1.79	1.72	1.13	1.78
$\eta_{exg,g}$ (%)	14.18	-	13.86	14.34	-	14.23	14.60	5.54	14.89	14.76	7.97	15.21	14.65	9.65	15.11
LCOE ($/(kW·h))	0.0482	-	0.0629	0.0434	-	0.0554	0.0409	0.1571	0.0503	0.0401	0.1056	0.0488	0.0397	0.0848	0.0481
(B) Case II															
	R290			**R152a**			**R600**			**R245fa**			**R601a**		
Parameters (unit)	**ORC**	**OFC**	**OFRC**	**ORC**	**OFC**	**OFRC**	**ORC**	**OFC**	**OFRC**	**ORC**	**OFC**	**OFRC**	**ORC**	**OFC**	**OFRC**
T_{eva} (°C)	91.7	-	91.7	79.69	-	81.5	78.56	-	80.01	78.6	-	79.92	78.08	-	79.49
T_3 (°C)	-	91.7	77.86	-	108.3	76.14	-	112	75.08	-	112	74.58	-	112	74.54
T_4 (°C)	-	71.36	71.86	-	81.4	65.94	-	78.92	63.48	-	78.66	62.27	-	77.84	61.61
W_{net} (kW)	1135.8	−136.51	1140.5	1027.5	354.50	1053.0	1032.9	592.63	1078.1	1045.0	704.99	1099.4	1029.6	786.13	1084.0
$\eta_{th,g}$ (%)	3.04	-	3.05	2.75	0.95	2.82	2.76	1.58	2.88	2.79	1.89	2.94	2.75	2.10	2.90
$\eta_{exg,g}$ (%)	21.52	-	21.61	19.47	6.72	19.95	19.57	11.23	20.43	19.80	13.36	20.83	19.51	14.90	20.54
LCOE ($/(kW·h))	0.0383	-	0.0498	0.0326	0.1318	0.0407	0.0303	0.0741	0.0368	0.0297	0.0603	0.0359	0.0293	0.0522	0.0352
(C) Case III															
	R290			**R152a**			**R600**			**R245fa**			**R601a**		
Parameters (unit)	**ORC**	**OFC**	**OFRC**	**ORC**	**OFC**	**OFRC**	**ORC**	**OFC**	**OFRC**	**ORC**	**OFC**	**OFRC**	**ORC**	**OFC**	**OFRC**
T_{eva} (°C)	91.68	-	90.4	108.3	-	108.3	90.28	-	93	90.29	-	93.16	89.05	-	91.77
T_3 (°C)	-	91.7	91.7	-	108.3	87.66	-	132	83.73	-	132	83.31	-	132	82.88
T_4 (°C)	-	71.36	89.12	-	81.4	78.19	-	92.52	70.17	-	91.92	68.95	-	89.62	67.58
W_{net} (kW)	1983.2	−176.64	1911.4	1952.2	458.45	2034.2	1766.5	1266.2	1870.5	1788.0	1385.9	1907.6	1742.2	1446.1	1858.3
$\eta_{th,g}$ (%)	4.41	-	4.25	4.34	1.02	4.52	3.93	2.82	4.16	3.98	3.08	4.24	3.87	3.22	4.13
$\eta_{exg,g}$ (%)	27.00	-	26.02	26.58	6.24	27.69	24.05	17.24	25.47	24.34	18.87	25.97	23.72	19.69	25.30
LCOE ($/(kW·h))	0.0328	-	0.0363	0.0279	0.1149	0.0353	0.0247	0.0470	0.0301	0.0241	0.0415	0.0292	0.0238	0.0379	0.0286

Abbreviations: LCOE, levelized cost of electricity; OFC, organic flash cycle; OFRC, organic flash Rankine cycle; ORC, organic Rankine cycle.

constraints have been summarized in Table 10. The PSO tuning parameters are determined based on Ref.,[48] and to ensure that the system operates under reliable subcritical conditions, both the maximum evaporation temperature ($T_{eva,max}$) and the maximum heater outlet temperature ($T_{3,max}$) are limited to be at least 5°C lower than the critical temperature (T_{cr}) of the working fluid. In addition, the vapor quality (x) in the flash tank is set to be in the range of 0.1–0.9 to ensure the operational feasibility of the system.[28]

In this study, the optimization objective is set to search the maximum net electrical power output, which is equivalent to searching the maximum global thermal and exergy efficiencies. Table 11 shows the solved optimization results of the ORC, OFC and OFRC systems under three typical heat source conditions. It can be seen that for all three heat source conditions, the OFRC system can achieve larger net electrical power output and higher global efficiencies than the ORC and OFC systems (i.e., the OFRC system has a better thermodynamic performance than the two basic systems). Compared to the ORC system and OFRC system, the OFC system has the worst thermodynamic performance, and its thermodynamic performance is strongly affected by the working fluid used. For example, when the inlet temperature of the heat source is set to 100°C and R290 is used as the working fluid, the system's net electrical power output is even equal to −96.69 kW, which means that the electricity obtained from the generator is not enough to cover the mechanical work consumed by pumps at this time. Obviously, this is very unreasonable, and in this case, the use of R290 as the system working fluid should be avoided. It is found that with the increase in the critical temperature of the working fluid, the thermodynamic performance of the OFC system is getting better. Thus, it is concluded that the working fluids with high critical temperatures (such as R601a) are more suitable for the OFC system. However, for the ORC system and OFRC system, their best working fluids are not fixed and vary with the heat source condition. In this study, R245fa, R290, and R152a are considered to be the best working fluid for the OFRC system when the inlet temperature of the heat source is set to 100°C, 120°C, and 140°C, respectively.

The economic analysis results of Table 11 show that for all three heat source conditions, the ORC system can achieve the lowest specific power cost, while the OFC system always has the highest specific power cost. Besides, it is found that for all three low-temperature heat recovery systems, with the increase of the critical temperature of the working fluid, the specific power cost of the system is getting lower, as described in Section 4.2. Thus, it is concluded that the higher the critical temperature of the working fluid, the better the economic performance of the system. Overall, the OFC system is not recommended to be used for low-temperature heat recovery due to its poor thermo-economic performance. If users pay more attention to the thermodynamic performance of the system, the OFRC system will be a good option. And the ORC system will be the first choice when users are more concerned with the economic performance of the system.

5 | CONCLUSIONS

In this paper, a novel OFRC system is modeled and analyzed from the viewpoints of thermodynamics and economics. Five environmentally friendly organic fluids and three typical low-temperature heat source conditions are discussed during the parametric analysis and optimization process. The main conclusions drawn from this study are listed as follows:

(1) The OFRC system's biggest exergy loss is caused by the condenser, followed by the evaporator. About 70% and 30% of the specific power cost are caused by the capital investment cost and the operation and maintenance cost, respectively. Besides, more than 60% of the capital investment cost is used to purchase the LP and HP expanders.
(2) Compared to the evaporation temperature and heater outlet temperature, the flashing temperature has a smaller effect on the system performance, and under the same operating conditions, the working fluids with high critical temperatures can achieve higher cycle thermal efficiency and lower specific power cost, while the working fluids with low critical temperatures can achieve larger heat recovery ratio.
(3) The OFRC system can achieve a better thermodynamic performance than the ORC and OFC systems, and when the heat source's inlet temperature is set to 100°C, 120°C, and 140°C, R245fa, R290, and R152a are, respectively recommended as the best working fluid for the OFRC system.
(4) The thermo-economic performance of the OFC system is the worst and is greatly affected by the working fluid used. In addition, for all three systems, the higher the critical temperature of the working fluid, the lower the specific power cost of the system.
(5) The OFC system is not recommended to be used for low-temperature heat recovery due to its poor system performance. If users pay more attention to the thermodynamic performance of the system, the OFRC system will be a good option. And the ORC system will be the first choice when users are more concerned with the economic performance of the system.

NOMENCLATURE

SYMBOLS

a	acceleration coefficient
A	heat transfer area (m^2)
c	cost rate ($\$\ h^{-1}$)
C	cost ($)
ex	specific exergy ($kJ\ kg^{-1}$)
Ex	exergy flow rate (kW)
g	gravitational acceleration ($m\ s^{-2}$)
h	specific enthalpy ($kJ\ kg^{-1}$)
H	pump head (m)
I	exergy loss rate (kW)
j	interest rate
$\dot{m}$	mass flow rate ($kg\ s^{-1}$)
n	lifetime (year)
N	annual operating hours (h)
P	pressure (kPa)
Q	heat flow rate (kW)
$Rand$	random number
s	specific entropy ($kJ\ kg^{-1}\ K^{-1}$)
T	temperature (°C)
U	heat transfer coefficient ($kW\ m^{-2}\ K^{-1}$)
v	velocity vector
w	inertia weight
W	power (kW)
x	vapor quality
X	position vector

GREEK SYMBOLS

α	heat recovery ratio
β	exergy recovery ratio
γ	maintenance factor
η	efficiency
Δ	difference

SUBSCRIPTS

0	ambient conditions
con	condenser/condensation
cp	circulating pump
cv	control volume
cw	cooling water
eva	evaporator/evaporation
exp	expander
exg	exergy
ft	flash tank
g	global
gb	global best
hs	heat source
in	inlet
is	isentropic
m	mechanical
max	maximum
min	minimum
OM	operation and maintenance
out	outlet
p	pump
pb	personal best
pp	pinch point
rec	recyclable
ref	reference year
sup	superheated
th	thermal
tot	total

ACKNOWLEDGMENT

Qi Wang greatly acknowledges the financial support from the China Scholarship Council (CSC, No. 202006280024). Open Access funding enabled and organized by Projekt DEAL.

CONFLICT OF INTEREST

The authors declare no conflict of interest.

ORCID

Qi Wang http://orcid.org/0000-0001-6656-2899

REFERENCES

1. Ahmadi P, Dincer I, Rosen MA. Exergo-environmental analysis of an integrated organic Rankine cycle for trigeneration. *Energy Convers Manage*. 2012;64:447-453. doi:10.1016/j.enconman.2012.06.001
2. Quoilin S, Broek MVD, Declaye S, et al. Techno-economic survey of Organic Rankine Cycle (ORC) systems. *Renew Sustain Energy Rev*. 2013;22:168-186. doi:10.1016/j.rser.2013.01.028
3. Park B-S, Usman M, Imran M, et al. Review of Organic Rankine Cycle experimental data trends. *Energy Convers Manage*. 2018;173:679-691. doi:10.1016/j.enconman.2018.07.097
4. Zhai H, An Q, Shi L, et al. Categorization and analysis of heat sources for organic Rankine cycle systems. *Renew Sustain Energy Rev*. 2016;64:790-805. doi:10.1016/j.rser.2016.06.076
5. Mahmoudi A, Fazli M, Morad MR. A recent review of waste heat recovery by Organic Rankine Cycle. *Appl Therm Eng*. 2018;143:660-675. doi:10.1016/j.applthermaleng.2018.07.136
6. Zhang H-H, Xi H, He Y-L, et al. Experimental study of the organic rankine cycle under different heat and cooling conditions. *Energy*. 2019;180:678-688. doi:10.1016/j.energy.2019.05.072
7. Feng Y, Zhang Y, Li B, et al. Comparison between regenerative organic Rankine cycle (RORC) and basic organic Rankine cycle (BORC) based on thermoeconomic multi-objective optimization considering exergy efficiency and levelized energy cost (LEC). *Energy Convers Manage*. 2015;96:58-71. doi:10.1016/j.enconman.2015.02.045
8. Baccioli A, Antonelli M. Organic Flash Cycles: Off-design behavior and control strategies of two different cycle architectures for Waste Heat Recovery applications. *Energy Convers Manage*. 2018;157:176-185. doi:10.1016/j.enconman.2017.12.004

9. Dong B, Xu G, Luo X, et al. Analysis of the supercritical organic Rankine cycle and the radial turbine design for high temperature applications. *Appl Therm Eng*. 2017;123:1523-1530. doi:10.1016/j.applthermaleng.2016.12.123
10. Zhao L, Bao J. Thermodynamic analysis of organic Rankine cycle using zeotropic mixtures. *Appl Energy*. 2014;130:748-756. doi:10.1016/j.apenergy.2014.03.067
11. Smith IK. Development of the Trilateral Flash Cycle System: Part 1: Fundamental Considerations. *Proc Inst Mech Eng Part A J Power Energy*. 1993;207:179-194. doi:10.1243/PIME_PROC_1993_207_032_02
12. Ho T, Mao SS, Greif R. Comparison of the Organic Flash Cycle (OFC) to other advanced vapor cycles for intermediate and high temperature waste heat reclamation and solar thermal. *Energy*. 2012;42:213-223. doi:10.1016/j.energy.2012.03.067
13. Sun Q, Wang Y, Cheng Z, et al. Thermodynamic and economic optimization of a double-pressure organic Rankine cycle driven by low-temperature heat source. *Renew Energy*. 2020;147:2822-2832. doi:10.1016/j.renene.2018.11.093
14. Wang Q, Wu W, He Z. Thermodynamic analysis and optimization of a novel organic Rankine cycle-based micro-scale cogeneration system using biomass fuel. *Energy Convers Manage*. 2019;198:111803. doi:10.1016/j.enconman.2019.111803
15. Shu G, Yu G, Tian H, et al. Multi-approach evaluations of a cascade-Organic Rankine Cycle (C-ORC) system driven by diesel engine waste heat: Part A—thermodynamic evaluations. *Energy Convers Manage*. 2016;108:579-595. doi:10.1016/j.enconman.2015.10.084
16. Rashwan SS, Dincer I, Mohany A. Analysis and assessment of cascaded closed loop type organic Rankine cycle. *Energy Convers Manage*. 2019;184:416-426. doi:10.1016/j.enconman.2018.12.089
17. Zhang C, Lin J, Tan Y. A theoretical study on a novel combined organic Rankine cycle and ejector heat pump. *Energy*. 2019;176:81-90. doi:10.1016/j.energy.2019.03.190
18. Li Z, Huang R, Lu Y, et al. Analysis of a combined trilateral cycle - organic Rankine cycle (TLC-ORC) system for waste heat recovery. *Energy Proc*. 2019;158:1786-1791. doi:10.1016/j.egypro.2019.01.421
19. Schuster A, Karellas S, Aumann R. Efficiency optimization potential in supercritical Organic Rankine Cycles. *Energy*. 2010;35:1033-1039. doi:10.1016/j.energy.2009.06.019
20. Pan L, Wang H, Shi W. Performance analysis in near-critical conditions of organic Rankine cycle. *Energy*. 2012;37:281-286. doi:10.1016/j.energy.2011.11.033
21. Chen H, Goswami DY, Stefanakos EK. A review of thermodynamic cycles and working fluids for the conversion of low-grade heat. *Renew Sustain Energy Rev*. 2010;14:3059-3067. doi:10.1016/j.rser.2010.07.006
22. Sadeghi M, Nemati A, Ghavimi A, et al. Thermodynamic analysis and multi-objective optimization of various ORC (organic Rankine cycle) configurations using zeotropic mixtures. *Energy*. 2016;109:791-802. doi:10.1016/j.energy.2016.05.022
23. Zhai H, An Q, Shi L. Zeotropic mixture active design method for organic Rankine cycle. *Appl Therm Eng*. 2018;129:1171-1180. doi:10.1016/j.applthermaleng.2017.10.027
24. Bamorovat Abadi G, Kim KC. Investigation of organic Rankine cycles with zeotropic mixtures as a working fluid: advantages and issues. *Renew Sustain Energy Rev*. 2017;73:1000-1013. doi:10.1016/j.rser.2017.02.020
25. Wang Q, Wu W, He Z, et al. Analysis of the intake process and its influence on the performance of a two-phase reciprocating expander. *Appl Therm Eng*. 2019;160:113943. doi:10.1016/j.applthermaleng.2019.113943
26. Yari M, Mehr AS, Zare V, et al. Exergoeconomic comparison of TLC (trilateral Rankine cycle), ORC (organic Rankine cycle) and Kalina cycle using a low grade heat source. *Energy*. 2015;83:712-722. doi:10.1016/j.energy.2015.02.080
27. Bianchi G, Kennedy S, Zaher O, et al. Numerical modeling of a two-phase twin-screw expander for Trilateral Flash Cycle applications. *Int J Refrig*. 2018;88:248-259. doi:10.1016/j.ijrefrig.2018.02.001
28. Wang Q, Wu W, Li D, et al. Thermodynamic analysis and optimization of four organic flash cycle systems for waste heat recovery. *Energy Convers Manage*. 2020;221:113171. doi:10.1016/j.enconman.2020.113171
29. Ahmadi M, Vahaji S, Arbab Iqbal M, et al. Experimental study of converging-diverging nozzle to generate power by Trilateral Flash Cycle (TFC). *Appl Therm Eng*. 2019;147:675-683. doi:10.1016/j.applthermaleng.2018.10.116
30. Baccioli A, Antonelli M, Desideri U. Technical and economic analysis of organic flash regenerative cycles (OFRCs) for low temperature waste heat recovery. *Appl Energy*. 2017;199:69-87. doi:10.1016/j.apenergy.2017.04.058
31. Ho T, Mao SS, Greif R. Increased power production through enhancements to the Organic Flash Cycle (OFC). *Energy*. 2012;45:686-695. doi:10.1016/j.energy.2012.07.023
32. Chen LX, Hu P, Sheng CC, et al. Thermodynamic analysis of three ejector based organic flash cycles for low grade waste heat recovery. *Energy Convers Manage*. 2019;185:384-395. doi:10.1016/j.enconman.2019.02.016
33. Meng D, Liu Q, Ji Z. Performance analyses of regenerative organic flash cycles for geothermal power generation. *Energy Convers Manage*. 2020;224:113396. doi:10.1016/j.enconman.2020.113396
34. Meng D, Liu Q, Ji Z. Effects of two-phase expander on the thermoeconomics of organic double-flash cycles for geothermal power generation. *Energy*. 2022;239(Part D):122346. doi:10.1016/j.energy.2021.122346
35. Khosravi H, Salehi GR, Azad MT. Design of structure and optimization of organic Rankine cycle for heat recovery from gas turbine: the use of 4E, advanced exergy and advanced exergoeconomic analysis. *Appl Therm Eng*. 2019;147:272-290. doi:10.1016/j.applthermaleng.2018.09.128
36. Li D, He Z, Wang Q, et al. Thermodynamic analysis and optimization of a partial evaporating dual-pressure organic rankine cycle system for low-grade heat recovery. *Appl Therm Eng*. 2021;185:116363. doi:10.1016/j.applthermaleng.2020.116363
37. Lee HY, Park SH, Kim KH. Comparative analysis of thermodynamic performance and optimization of organic flash cycle (OFC) and organic Rankine cycle (ORC). *Appl Therm Eng*. 2016;100:680-690. doi:10.1016/j.applthermaleng.2016.01.158
38. Hu S, Li J, Yang F, et al. Thermodynamic analysis of serial dual-pressure organic Rankine cycle under off-design conditions. *Energy Convers Manage*. 2020;213:112837. doi:10.1016/j.enconman.2020.112837

39. Ibarra M, Rovira A, Alarcón-Padilla D-C. Performance of an Organic Rankine Cycle with two expanders at off-design operation. *Appl Therm Eng*. 2019;149:688-701. doi:10.1016/j.applthermaleng.2018.12.083
40. Liu Q, Shen A, Duan Y. Parametric optimization and performance analyses of geothermal organic Rankine cycles using R600a/R601a mixtures as working fluids. *Appl Energy*. 2015;148:410-420. doi:10.1016/j.apenergy.2015.03.093
41. Jang Y, Lee J. Optimizations of the organic Rankine cycle-based domestic CHP using biomass fuel. *Energy Convers Manage*. 2018;160:31-47. doi:10.1016/j.enconman.2018.01.025
42. Chuang W, Shun-sen W, Jun L. Exergoeconomic analysis and optimization of a combined supercritical carbon dioxide recompression Brayton/organic flash cycle for nuclear power plants. *Energy Convers Manage*. 2018;171:936-952. doi:10.1016/j.enconman.2018.06.041
43. Xurong W, Yiping D. Exergoeconomic analysis of utilizing the transcritical CO_2 cycle and the ORC for a recompression supercritical CO_2 cycle waste heat recovery: A comparative study. *Appl Energy*. 2016;170:193-207. doi:10.1016/j.apenergy.2016.02.112
44. Mohammadi K, Ellingwood K, Powell K. A novel triple power cycle featuring a gas turbine cycle with supercritical carbon dioxide and organic Rankine cycles: Thermoeconomic analysis and optimization. *Energy Convers Manage*. 2020;220:113123. doi:10.1016/j.enconman.2020.113123
45. MATLAB. *MATLAB/Simulink*. MathWorks; 2021. https://www.mathworks.com/products/matlab.html.
46. Lemmon EW, Huber ML, McLinden MO. *NIST Standard Reference Database 23: Reference Fluid Thermodynamic and Transport Properties REFPROP*. National Institute of Standards and Technology, Standard Reference Data Program; 2010.
47. Zeting Y, Ruizhi S, Chunyu F. Thermodynamic analysis and multi-objective optimization of a novel power generation system driven by geothermal energy. *Energy*. 2020;199:117381. doi:10.1016/j.energy.2020.117381
48. Wang Q, Liu C, Luo R, et al. Thermo-economic analysis and optimization of the very high temperature gas-cooled reactor-based nuclear hydrogen production system using copper-chlorine cycle. *Int J Hydrogen Energy*. 2021;46:31563-31585. doi:10.1016/j.ijhydene.2021.07.060

How to cite this article: Wang Q, Macián-Juan R, Li D. Analysis and assessment of a novel organic flash Rankine cycle (OFRC) system for low-temperature heat recovery. *Energy Sci Eng*. 2022;10:3023-3043. doi:10.1002/ese3.1186